ELSEVIER

Solid State Ionics 156 (2003) 309–318

SOLID STATE IONICS

www.elsevier.com/locate/ssi

Structure and physical property changes of de-lithiated spinels for $Li_{1.02-x}Mn_{1.98}O_4$ after high-temperature storage

Hironori Kobayashi[a,*], Hikari Sakaebe[a], Kenichi Komoto[a], Hiroyuki Kageyama[a], Mitsuharu Tabuchi[a], Kuniaki Tatsumi[a], Tomoko Kohigashi[b], Masao Yonemura[b], Ryoji Kanno[c], Takashi Kamiyama[d]

[a] *Special Division of Green Life Technology, National Institute of Advanced Industrial Science and Technology (AIST), 1-8-31 Midorigaoka, Ikeda, Osaka 563-8577, Japan*

[b] *Department of Chemistry, Graduate School of Science and Technology, Kobe University, Rokko-dai, Nada, Kobe 657-8501, Japan*

[c] *Department of Electronic Chemistry, Interdisciplinary Graduate School of Science and Engineering, Tokyo Institute of Technology, Nagatsuta, Midori, Yokohama 226-8502, Japan*

[d] *Institute of Materials Structure Science, High Energy Accelerator Research Organization (KEK), Oho, Tsukuba, Ibaraki 305-0801, Japan*

Received 15 February 2002; received in revised form 24 July 2002; accepted 28 July 2002

Abstract

High-temperature storage of the lithium manganese spinel cathode was examined for $Li_{1.02-x}Mn_{1.98}O_4$ using 1 M $LiPF_6$ in EC:DEC (1:1) electrolyte solution. The structure, magnetic properties, and valence state of Mn were determined before and after the storage using Mn *K*-edge XANES, X-ray diffraction, SQUID, ICP spectroscopy, and electrochemical measurements. After the storage at 80 °C for 6 days, single-phase property was observed at $x=0$ and 0.96 in $Li_{1.02-x}Mn_{1.98}O_4$, while multi-phase property was observed between the compositions, $x=0.18$ and 0.63. Shallow de-lithiated region near $x=0.18$ was easily affected by the storage; the $Li/Li_{1.02-x}Mn_{1.98}O_4$ cell showed large capacity failure from 111 to 40 mAh/g after the storage, which corresponded to the phase transition with the increase in the valence state of Mn after the storage. Magnetic measurement was found to be quite sensitive and effective to detect the subtle structural changes caused by the high-temperature storage.

PACS: 84.60.D

Keywords: Lithium manganese spinel; Cathode materials; Mn dissolution; Mn *K*-edge XANES measurement; SQUID measurement

1. Introduction

Lithium manganese spinel is one of the most promising cathode materials for lithium secondary battery [1]. The cycling performance using the spinel cathode has been extremely improved for the cells operated at room temperature [2], while the capacity failure after the storage at elevated temperature is one of the major problems to be solved. The dissolution of manganese ions from the spinel cathode was undoubtedly considered as a trigger of the damage to the battery systems using $LiPF_6$ electrolyte. In addition, several mechanisms followed by the dissolution have been proposed [3–14]: (a) theoretical capacity change

* Corresponding author. Tel.: +81-727-51-9649; fax: +81-727-51-9609.

E-mail address: hironori-kobayashi@aist.go.jp (H. Kobayashi).

0167-2738/03/$ - see front matter © 2003 Elsevier Science B.V. All rights reserved.
PII: S0167-2738(02)00692-6

caused by a shift of the spinel to a Li-excess composition, (b) the appearance of an electrochemical inactive phase such as Li_2MnO_3, (c) surface morphology change, (d) Mn deposition on the surface of the negative electrode. The compositions, structure, and Mn valence state of the spinel are affected by the Mn dissolution under the high-temperature storage. However, those changes have not been clearly understood, partly because its structural changes are very small, and because the decrease in crystallinity makes it difficult to determine the changes by diffraction technique. We tried to use magnetic properties as a probe to detect the subtle structural changes.

Magnetic properties of the spinels have been investigated previously. For example, Tabuchi et al. [15] reported the changes in the effective magnetic moment and the Weiss temperature with increasing Mn oxidation state in the defect $Li_{1-\delta}Mn_{2-\delta}O_4$ spinel. Masquelier et al. [16] reported that the oxidation of Mn^{3+} to Mn^{4+} state resulted in a progressive change from the antiferromagnetic ($LiMn_2O_4$, $\theta = -266$ K) to ferromagnetic ($Li_4Mn_5O_{12}$, $\theta = +40$ K) behavior in the $LiMn_2O_4$–$Li_4Mn_5O_{12}$ system. Shimakawa et al. [17] also reported the change from the antiferromagnetic to ferromagnetic behavior with increasing Mn^{4+}/Mn^{3+} ratio in $Li_{1+x}Mn_{2-x}O_4$. Furthermore, Endres et al. [18] reported the appearance of antiferromagnetic transition at 40 K with increasing oxygen vacancy in $LiMn_2O_{4-y}$. These magnetic measurements give us information on the valence state of Mn as well as the structures of lithium manganese spinels.

In this study, the stability of de-lithiated samples $Li_{1.02-x}Mn_{1.98}O_4$ using H_2SO_4 [19] was examined in the electrolyte at elevated temperature, and the changes in magnetic behavior were clarified. The magnetic measurement was used as a main tool to obtain information on the valence states of Mn and structural changes. Furthermore, the relationships between the storage conditions, structural changes, and their electrochemical properties were discussed based on the magnetic data.

2. Experimental

$Li_{1.02}Mn_{1.98}O_4$ was prepared by heating appropriate molar ratios of Li_2CO_3 (Wako) and MnO_2

Table 1
The compositions and lattice parameters of the samples examined in the present study

Samples	Li/Mn ratio	Calculated composition	Lattice parameters	O(x)	R_{wp}	R_I	S(R_{wp}/R_e)	Ratio of phases
Ab (host material)	0.516	$Li_{1.02}Mn_{1.98}O_4$	8.23928(5)	0.26194(12)	10.62	2.30	1.31	
Bb (treated by 0.072 N H_2SO_4)	0.423	$Li_{0.84}Mn_{1.98}O_4$	8.22258(8)	0.26382(19)	14.11	5.01	1.29	
Cb (treated by 0.144 N H_2SO_4)	0.341	$Li_{0.68}Mn_{1.98}O_4$	8.18886(10)	0.26293(19)	13.68	3.10	1.21	
Db (treated by 0.216 N H_2SO_4)	0.276	$Li_{0.55}Mn_{1.98}O_4$	8.15833(10)	0.2634(2)	14.94	4.12	1.26	
Eb (treated by 0.288 N H_2SO_4)	0.199	$Li_{0.39}Mn_{1.98}O_4$	8.13100(17)	0.2617(2)	15.49	3.79	1.45	0.89
			8.0619(8)	0.2669(12)		3.96		0.11
Fb (treated by 0.576 N H_2SO_4)	0.038	$Li_{0.08}Mn_{1.98}O_4$	8.04194(6)	0.26333(18)	16.17	8.43	1.43	
Aa (after storage of sample Ab)	0.529	Single phase	8.23131(11)	0.26262(17)	12.94	3.00	1.59	
Ba (after storage of sample Bb)	0.443	Multi phases	8.1191(2)<Ba–S>	0.2598(2)	15.14	4.20	1.47	0.86
			8.211(2)<Ba–L>	0.2610(15)		4.00		0.14
Ca (after storage of sample Cb)	0.467	Multi phases	8.078(4)	0.2447(15)	14.71	8.22	1.42	0.27
			8.1537(4)	0.2623(3)		6.81		0.62
			8.2285(13)	0.269(2)		6.48		0.10
Da (after storage of sample Db)	0.384	Multi phases	8.0805(16)	0.246(6)	14.75	5.59	1.42	0.02
			8.1145(4)	0.2593(2)		5.05		0.79
			8.152(16)	0.266(2)		5.05		0.19
			+ Li_2MnO_3					–
Ea (after storage of sample Eb)	0.345	Multi phases	8.0579(4)	0.2612(4)	17.59	7.08	1.47	0.58
			8.1257(6)	0.2565(6)		6.89		0.42
			+ Li_2MnO_3					–
Fa (after storage of sample Fb)	0.152	Single phase	8.04290(6)	0.2636(2)	15.46	8.05	1.57	

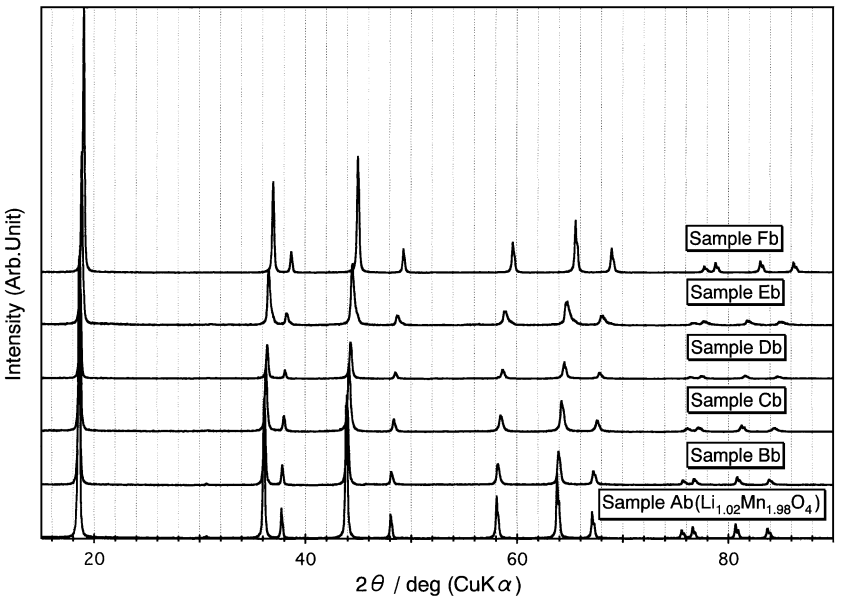

Fig. 1. X-ray diffraction patterns for $Li_{1.02-x}Mn_{1.98}O_4$ treated in H_2SO_4 for 9 h.

(CMD, Chuo-Denki Kogyo). The raw materials were weighed, mixed, pelletized, and pre-fired in air at 673 K for 48 h and were then fired in air at 973 K for 48 h. Lithium-deficient spinels were synthesized chemically by the treatment of 7.333 g of $Li_{1.02}Mn_{1.98}O_4$ in 200 ml H_2SO_4 (0.072–0.576 N) for 9 h. High-temperature storage experiments were examined in 1 M $LiPF_6$ in EC:DEC (1:1) electrolyte solution (Tomiyama Petrochemical, battery grade). About 3.5 g of samples was kept in 8.6 g of electrolyte at 80 °C for 6 days. The samples were washed by DEC and dried under vacuum at room temperature. The Li/Mn ratios were determined by ICP spectroscopy.

The Mn *K*-edge XANES spectra were measured by transmission mode with a laboratory type X-ray spectrometer, EXAC-820 (Technos) at 293 K. The X-ray generator with a Mn rotating anode and LaB_6 cathode was operated with a voltage of 20 kV and a current of 200 mA. The incident X-ray beam was monochromatized with a Ge(400) Johansson curved crystal for XANES measurement. The intensity of the X-ray beam was measured by a sealed proportional counter filled with 25% Ar and 75% N_2 gases for the incident X-ray and by a solid-state detector for the transmitted X-ray. The monochromator angle was calibrated with a characteristic Mn X-ray line for each measurement. XANES spectra were normalized at 6.65 keV. The Mn *K*-edge energy was defined as the energy at the half height of the Mn *K*-edge absorption edge.

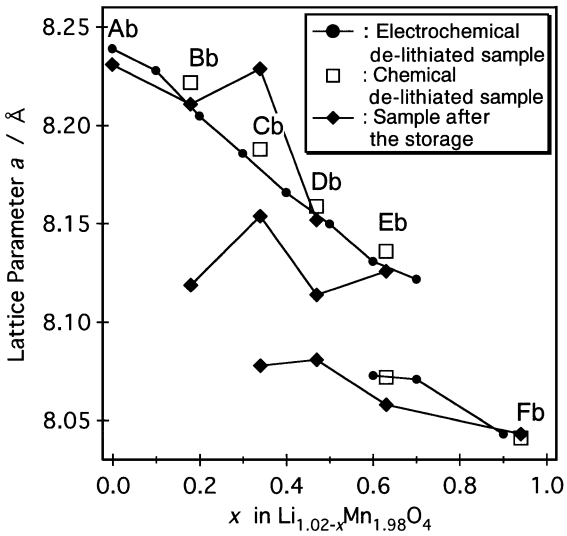

Fig. 2. Composition dependence of the lattice parameters for the samples de-lithiated by electrochemical (●), chemical treatment (□), and stored (♦) in electrolyte solution at 80 °C.

Table 2
K-edge and peak top energy in XANES spectra for the samples delithiated by chemical treatment (a), and the samples after stored in the electrolytes at high-temperatures (b)

(a)

Samples	Ab (eV)	Bb (eV)	Cb (eV)	Db (eV)	Eb (eV)	Fb (eV)
K-edge energy	6548.32	6548.43	6549.00	6549.08	6549.25	6550.38
Peak top energy	6556.0	6556.0	6556.5	6556.5	6556.5	6557.5

(b)

Samples	Aa (eV)	Ba (eV)	Ca (eV)	Da (eV)	Ea (eV)	Fa (eV)
K-edge energy	6548.07	6548.43	6548.08	6548.51	6548.18	6549.67
Peak top energy	6556.0	6557.0	6557.0	6557.0	6557.0	6557.5

X-ray diffraction (XRD) patterns of the powdered samples were obtained with an X-ray diffractometer (Rigaku Rotaflex/Rint-TTR) with Cu*K*α radiation. The diffraction data were collected for 2 s at each 0.02° step width over a 2θ range from 15° to 120°. The structural parameters were refined by Rietveld analysis using the computer program RIETAN97-beta [20]. The initial structural parameters were used from the refinement results of neutron diffraction data [21,22].

Temperature dependence and magnetic field dependence of the magnetization were measured by a SQUID magnetometer (Quantum Design, MPMS2) between 5 and 300 K. The sign and magnitude of the applied magnetic field were determined with a granular Pb metal. The magnetization was measured after cooling in zero field, and then measured again down to 5 K in applied magnetic field.

Electrochemical intercalation and deintercalation were carried out using lithium cells with a coin-type configuration. The working electrode consisted of a mixture of 20-mg samples, 6.7-mg acetylene black, and 3.3-mg Teflon powder. The mixture was pressed into a tablet of 15-mm diameter under a pressure of 0.5 MPa. The counter electrode was a 16-mm-diameter and 0.2-mm-thickness disk of lithium metal. A microporous polypropylene sheet was employed as the separator. The electrolyte used in these cells was 1 M $LiClO_4$ in PC:DEC (1:1) electrolyte solution (Tomiyama Petrochemical, battery grade). The cells were constructed in an argon-filled glove box. The electrochemical measurements were carried out at room temperature after standing overnight under zero

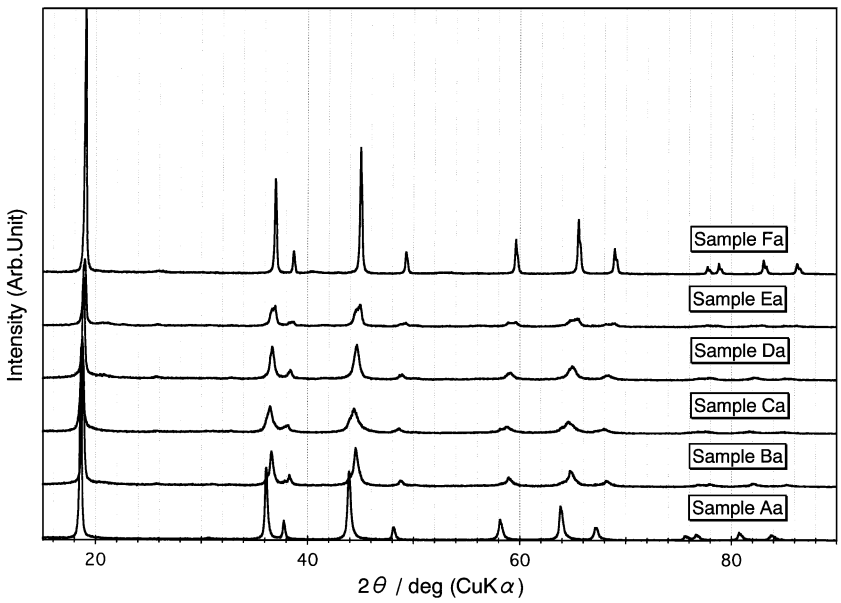

Fig. 3. X-ray diffraction patterns for $Li_{1.02-x}Mn_{1.98}O_4$ after the storage in electrolyte solution at 80 °C.

current flow. Cell properties were measured galvanostatically using BT2004 (Nagano).

3. Results and discussion

3.1. Synthesis and characterization of the spinel de-lithiated chemically

Table 1 summarizes the ICP and X-ray Rietveld results for the lithium-deficient spinels treated in H_2SO_4 using $Li_{1.02}Mn_{1.98}O_4$. The symbols, "Ab" and "Bb" to "Fb" represent the host and de-lithiated spinels, respectively. The lithium content of the de-lithiated samples was controlled by the concentration of H_2SO_4 from 0.072 to 0.576 N. Fig. 1 shows the XRD patterns for the host and the de-lithiated samples. Single-phase property was obtained by H_2SO_4 treatment with the concentrations, 0.072–0.216 and 0.576 N, while multi-phase property was obtained by the treatment of 0.288 N. ICP results showed the decrease of Li/Mn ratios from 0.42 to 0.04 with increasing H_2SO_4 concentration from 0.072 to 0.576 N. The lattice parameters of these spinels were refined by the Rietveld analysis. Fig. 2 shows the composition dependence of lattice parameters for the samples de-lithiated chemically, together with the data obtained for the samples de-lithiated electrochemically in the present study. The lattice parameters decreased from "Bb" to "Fb" with the increase of the H_2SO_4 content, through the two-phase region of "Eb". These parameters and the lithium contents were well consistent with our results of the de-lithiated samples obtained by the charge of lithium cell.

Table 2 summarizes the Mn *K*-edge energies for $Li_{1.02-x}Mn_{1.98}O_4$. The continuous shift of Mn *K*-edge absorption energy to higher energy from "Ab" to "Fb" indicated that the average valence state of Mn increased with decreasing Li content from $x=0$ to 0.94, through the two-phase region of "Eb".

3.2. XRD and XANES results

High-temperature storage in the electrolytes was examined using the samples de-lithiated chemically. The samples "Ab" to "Fb" were kept in the electrolyte at 80 °C for 6 days. The samples after the storage were represented as "Aa" to "Fa", where "a" indicates the samples after the storage. The notation from "A" to "F" corresponds to the concentration of H_2SO_4 used for the de-lithiation. Fig. 3 shows the XRD patterns for the samples after the storage. The XRD peaks became broad with the storage except the sample "Fa". Single-phase property was observed for the samples with the initial composition "Aa", and with the deep charged state "Fa", while multi-phase property was observed for the samples with shallow and middle charged state, "Ba" to "Ea". The samples

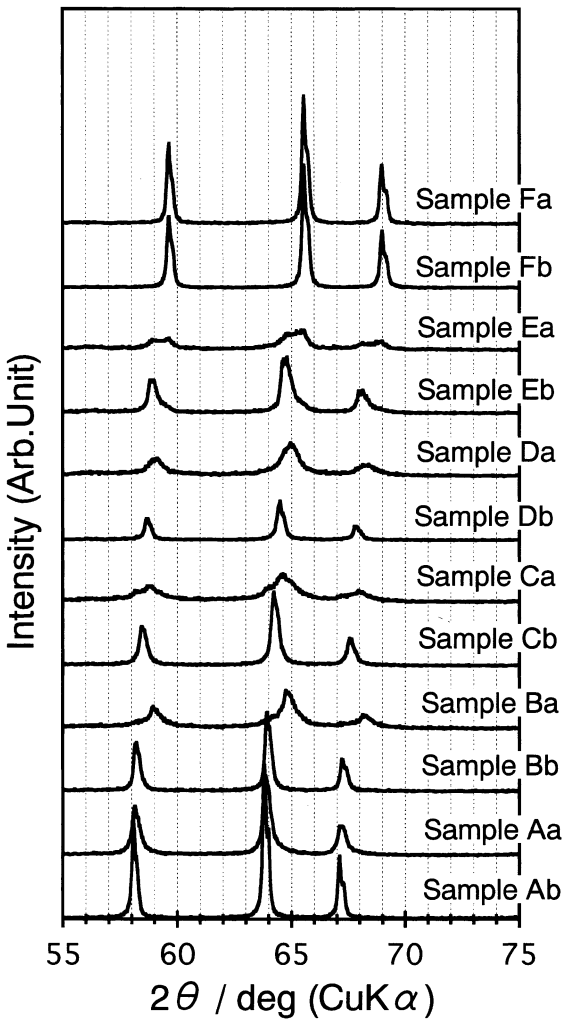

Fig. 4. X-ray diffraction patterns for $Li_{1.02-x}Mn_{1.98}O_4$ before and after the storage in electrolyte solution at 80 °C.

"Ba" to "Ea" are composed of two (or three) phases with larger and smaller lattice parameters, which was indicated by the change in peak position shown in Fig. 4. The sample "Ba" showed the large shift of the peak position to higher angles, indicating the existence of Mn^{4+}-rich spinel as a main phase. The ICP results showed the increase of Li/Mn ratio after the storage, indicating the dissolution of Mn from the spinel structure.

Fig. 5 shows the Mn *K*-edge XANES spectra for $Li_{1.02-x}Mn_{1.98}O_4$ before and after the storage. After the storage, the peak edge shift to lower energy was observed except the sample "Ba", indicating the increase in Mn^{3+} component, while the peak top shift to higher energy was observed for samples "Aa" to "Da", indicating the increase in Mn^{4+} component. These numerical data are shown in Table 2. These changes in Mn *K*-edge absorption energy reflected the composition shift from single-phase $Li_{1.02-x}Mn_{1.98}O_4$ to two (three) phases with Mn^{3+} and Mn^{4+}-rich composition after the storage. Especially, the appearance of Mn^{4+}-rich spinel was clarified by the profile change from sample "Bb" to "Ba".

The lattice parameter of the sample "Ab" decreased with the storage from 8.238 to 8.231 Å for "Aa", while the lattice parameter of the sample "Fb" increased from 8.042 to 8.043 Å for "Fa". These results are consistent with the XANES results that the increase in the Mn^{4+} component was observed for the sample "Aa", while the increase in the Mn^{3+} component was found for the sample "Fa".

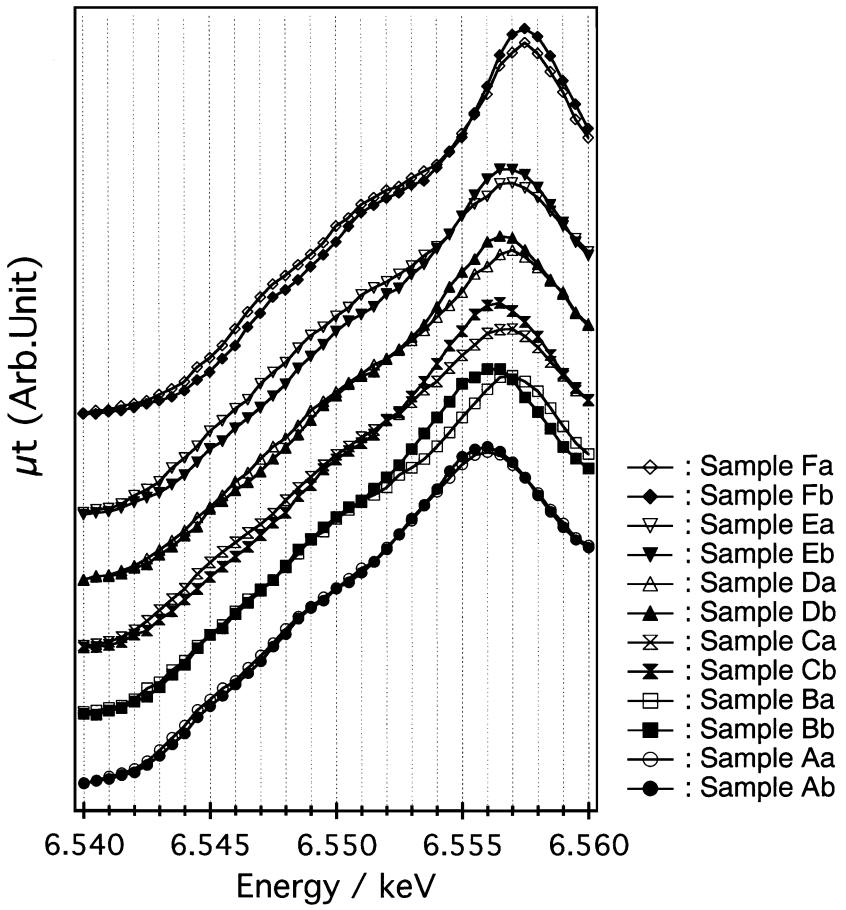

Fig. 5. Mn *K*-edge XANES spectra for $Li_{1.02-x}Mn_{1.98}O_4$ before and after the storage in electrolyte solution at 80 °C.

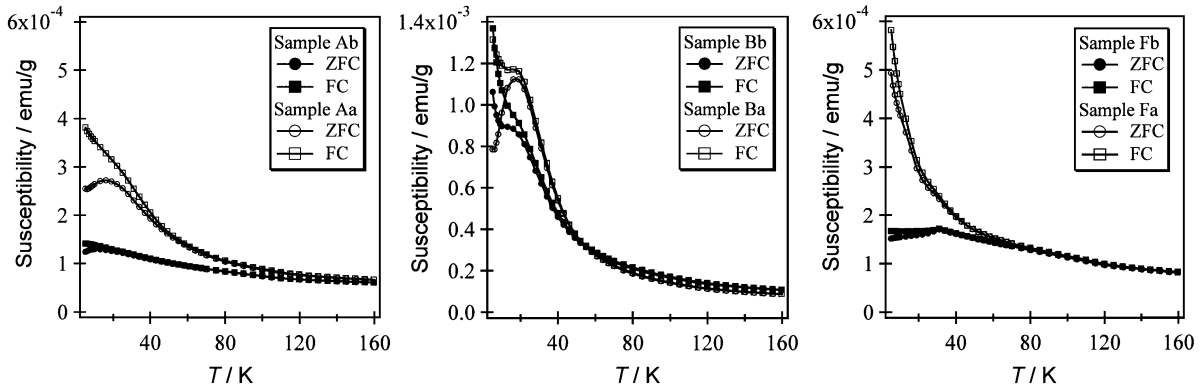

Fig. 6. Temperature dependence of the susceptibility for $Li_{1.02-x}Mn_{1.98}O_4$ before and after the storage in electrolyte solution at 80 °C.

3.3. Magnetic properties

Magnetic susceptibility was measured for the samples "Ab", "Bb", "Fb", "Aa", "Ba", and "Fa". Fig. 6 shows the temperature dependence of magnetic susceptibility, χ, in the range of 5–300 K. The spin-glass-like behavior with a cusp around 10 K was observed for the sample "Ab", and the abrupt increase in the magnetic susceptibility was observed below 40 K for the sample "Bb". The sample "Fb" showed the cusp around 30 K. The shift of the cusp to higher temperatures was observed with the decrease in lithium content from the samples "Ab" to "Fb". After the storage, the susceptibility increased and the cusp became sharp for the samples "A" to "E", while the cusp around 30 K disappeared for the sample "Fa". The increase in the ferromagnetic component that originated from the Mn^{4+}–O–Mn^{4+} interaction was indicated by the increase in the susceptibility for all the samples.

All the samples show the temperature-dependent susceptibilities with no magnetic ordering down to 180 K. The effective magnetic moment (μ_{eff}) was calculated using the equation $\chi_m^{-1}=(T-\theta)/C_m$ (C_m: Curie constant, θ: Weiss temperature) from the data in the temperature region of 180–300 K. Table 3 summarizes the magnetic parameters of μ_{eff} and θ. The theoretical effective moment of 4.37 and 3.87 μ_B was expected for $Li_{1.02}Mn_{1.98}O_4$ and $Li_{0.08}Mn_{1.98}O_4$, respectively, from mixed valence state consisting of Mn^{3+} ($S=2$, 4.90 μ_B) in the high-spin state and Mn^{4+} ($S=3/2$, 3.87 μ_B), assuming spin-only contribution for the magnetic moment. These values were in good agreement with the values of 4.37 and 3.77 μ_B determined for the samples "Ab" and "Fb", respectively. For the sample "Bb", the μ_{eff} value increased and the θ value decreased with the deintercalation of lithium from $Li_{1.02}Mn_{1.98}O_4$. After the storage, both the μ_{eff} and θ values decreased for all the samples. The decrease in the μ_{eff} value indicates that the valence state of Mn ions increased after the storage.

Fig. 7 shows the applied field (H) dependence of magnetization (M) before and after the storage. In these series, the magnetization increases after the storage. Particularly, a large difference in the H–M curve was observed between the samples "Bb" and "Ba". The increase in the ferromagnetic component that originated from the Mn^{4+}–O–Mn^{4+} interaction was indicated by the increase in the hysteresis for the sample "Ba". These results indicated that the sample "Bb" was easily affected by the storage and changed to a spinel with a Mn^{4+}-rich composition.

Table 3
Magnetic parameters for samples before and after the storage in electrolyte

Samples before the storage	Ab	Bb	Fb
Magnetic effective moment (μ_{eff})	4.37 μ_B	4.19 μ_B	3.77 μ_B
Weiss constant (θ)	−259 K	−64 K	−84 K
Samples after the storage	**Aa**	**Ba**	**Fa**
Magnetic effective moment (μ_{eff})	4.31 μ_B	3.77 μ_B	3.70 μ_B
Weiss constant (θ)	−215 K	−64 K	−77 K

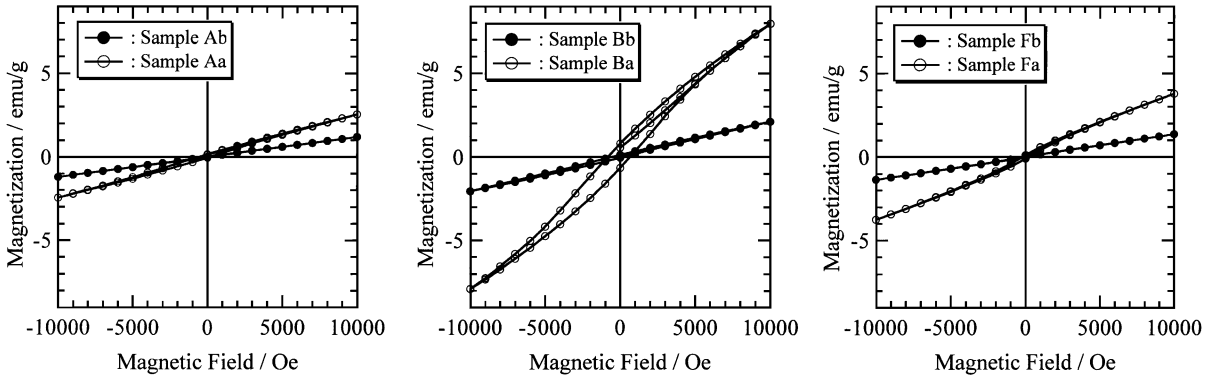

Fig. 7. Magnetic field dependence of the magnetization for $Li_{1.02-x}Mn_{1.98}O_4$ before and after the storage in electrolyte solution at 80 °C.

3.4. Electrochemical properties

Table 4 summarizes the discharge capacity and the capacity ratios, (the capacity after the storage)/(the capacity before the storage), for the samples "Ab", "Bb", "Fb", and "Aa", "Ba", "Fa". The $Li/Li_{1.02}Mn_{1.98}O_4$ (sample "Ab") cell showed the capacity of 129 mAh/g, while capacity failure from 129 to 101 mAh/g was observed for the sample "Aa" after the storage at 80 °C. The large capacity failure from 111 to 40 mAh/g and from 121 to 79 mAh/g was observed for the sample "Ba" and "Fa", respectively. The large capacity failure of the sample "Ba" corresponds to the significant changes in the composition and properties observed by our XRD, XANES, and magnetic measurements.

3.5. Discussion

The de-intercalated phase, $Li_{0.84}Mn_{1.98}O_4$ (sample "Bb"), changed significantly in the electrolyte solution containing $LiPF_6$ at 80 °C, and this indicated that the phase is the most unstable among the de-intercalated phases. The composition of the phase $Li_{0.84}Mn_{1.98}O_4$ was represented as $[Li_{0.82}\square_{0.18}][Li_{0.02}Mn_{1.98}]O_4$ (□: cation vacancy), which corresponds to the shallow charge state in the cathode materials. The composition of the sample "Ba" was determined from the ICP results to be $Li_{0.84}Mn_{1.90}O_4$, assuming that only Mn ions dissolved into the electrolyte solution at 80 °C. The observed capacity of 40 mAh/g was much smaller than the capacity of 104 mAh/g calculated from $Li_{0.84}Mn_{1.90}O_4$.

Table 4
Discharge capacity and the ratios of the capacity (the capacity after the storage/the capacity before the storage)

Composition (before)	Capacity (before) (mAh/g)	Capacity (after) (mAh/g)	Ratio
$Li_{1.02}Mn_{1.98}O_4$	129 (sample Ab)	101 (sample Aa)	0.78
$Li_{0.83}Mn_{1.98}O_4$	111 (sample Bb)	40 (sample Ba)	0.35
$Li_{0.07}Mn_{1.98}O_4$	121 (sample Fb)	79 (sample Fa)	0.65

After the storage, the sample "Bb" changed to the sample "Ba", which is composed of the main phase "Ba–S" with a smaller lattice parameter of 8.12 Å and a small amount of second-phase "Ba–L" with a larger lattice parameter of 8.21 Å. Comparing the characteristics of this main phase with the host "Ab" and de-lithiated samples "Bb" to "Db", the structure and properties are similar to those of the sample "Db" with a lattice parameter of 8.16 Å refined by XRD measurement, the manganese valence observed by the XANES experiments, and the magnetic behavior by magnetic measurement. In addition, the valence state of Mn ion with +3.77 for the sample "Ba–S" is close to that of Mn ion with +3.76 for the de-lithiated sample $Li_{0.55}Mn_{1.98}O_4$, although the influence of a small amount of the phase "Ba–L" on the structure and physical properties is taken into account. In Fig. 2, the phase with a lattice parameter of about 8.12 Å is strongly observed after the storage at 80 °C. These results indicate that the phase near the composition of $Li_{0.55}Mn_{1.98}O_4$ is more stable than the samples in the shallow charged state, and the Mn dissolution caused

the phase transition to a Mn^{4+}-rich phase with a disorder of Li ion conduction pathway.

$Li_{0.08}Mn_{1.98}O_4$ (sample "Fb") is represented as $[Li_{0.06}\square_{0.94}][Li_{0.02}Mn_{1.98}]O_4$ (□: cation vacancy), which corresponds to the fully charged state. Since the Mn valence state is 4+, there are two explanations of Mn dissolution: Li ions intercalate to structure during the storage, or Mn ions dissolved to electrolyte solution as MnO or Mn_3O_4. Assuming that the valence state of Mn ions was 4+ after the storage, the composition of the sample "Fa" was calculated to be $Li_{0.29}Mn_{1.93}O_4$. The observed capacity of 79 mAh/g was smaller than the capacity of 116 mAh/g calculated from $Li_{0.29}Mn_{1.93}O_4$. The ferromagnetic property of sample "Fa" indicates the appearance of a small amount of $Li_4Mn_5O_{12}$-related phase because $Li_4Mn_5O_{12}$ showed ferromagnetic property and much stronger susceptibility than λ-MnO_2. If we consider the existence of oxygen vacancy, the situation is more complex.

To clarify the stability of the de-lithiated samples, two samples were kept in vacuum oven. The sample "Bb" kept at 60 °C for 22 h showed peak broadening of X-ray diffraction patterns with the peak shift to lower angles, while the sample "Fb" did not show peak shift to lower angles until the storage temperature went up to 140 °C for 3 h.

Our samples obtained chemically by H_2SO_4 may be less stable than that obtained electrochemically. However, the decomposition of the sample "Bb" was observed even in air without the electrolyte solution containing $LiPF_6$. These results indicated that the sample "Bb", which corresponds to the shallow charge state, is substantially unstable and the decomposition is accelerated by Mn dissolution from the spinel structure. These results are in good agreement with what has been recently reported by Li et al. [23]. The detail structural analysis is currently underway using powder neutron diffraction measurements.

4. Conclusion

$Li_{1.02-x}Mn_{1.98}O_4$ was stored in 1 M $LiPF_6$ in EC:DEC (1:1) electrolyte solution at 80 °C for 6 days. For $Li_{0.84}Mn_{1.98}O_4$ (sample "Bb") with shallow charged state, multi-phase was observed in the XRD pattern and the shift of peak top to higher energy was observed in Mn *K*-edge XANES spectra after the storage. The increase in the ferromagnetic component was observed simultaneously. These results indicated that the increase in the Mn^{4+} component corresponded to the large capacity failure after the storage in the Li/$Li_{0.84}Mn_{1.98}O_4$ cell. The magnetic and XANES data indicated the valence state change and coordination situation of Mn ions. It was clarified that the de-intercalated phase, $Li_{0.84}Mn_{1.98}O_4$ (sample "Bb"), is the most unstable among the de-intercalated phases in the electrolyte solution containing $LiPF_6$ at 80 °C.

Acknowledgements

This work was partly supported by a Grant-in Aid for University and Society Collaboration (No. 12793004) from The Ministry of Education, Culture, Sports, Science and Technology of Japan.

References

[1] M. Tarascon, D. Guyomard, J. Electrochem. Soc. 138 (1991) 2864.
[2] Y. Xia, M. Yoshio, J. Electrochem. Soc. 143 (1996) 825.
[3] R.J. Gummow, A. de Kock, M.M. Thackeray, Solid State Ionics 69 (1994) 59.
[4] Y. Gao, J.R. Dahn, J. Electrochem. Soc. 143 (1996) 1783.
[5] O. Schilling, J.R. Dahn, J. Electrochem. Soc. 145 (1998) 569.
[6] A. Blyr, C. Sigala, G. Amatucci, D. Guyomard, Y. Chabre, J.M. Tarascon, J. Electrochem. Soc. 145 (1998) 194.
[7] D.H. Jang, S.M. Oh, J. Electrochem. Soc. 144 (1997) 3342.
[8] T. Inoue, M. Sano, J. Electrochem. Soc. 145 (1998) 3704.
[9] H. Huang, C.A. Vincent, P.G. Bruce, J. Electrochem. Soc. 146 (1999) 481.
[10] A.D. Pasquier, A. Blyr, P. Courjal, D. Larcher, G. Amatucci, B. Geranand, J.M. Tarascon, J. Electrochem. Soc. 146 (1999) 428.
[11] Y. Terada, Y. Nishiwaki, I. Nakai, F. Nishikawa, J. Power Sources 97–98 (2001) 420.
[12] H. Yamane, T. Inoue, M. Fujita, M. Sano, J. Power Sources 99 (2001) 60.
[13] S. Ma, H. Noguchi, M. Yoshio, K. Shizuka, J. Power Sources 97–98 (2001) 385.
[14] T. Aoshima, K. Okahara, C. Kiyohara, K. Shizuka, J. Power Sources 97–98 (2001) 377.
[15] M. Tabuchi, C. Masquelier, H. Kobayashi, R. Kanno, Y. Kobayashi, T. Akai, Y. Maki, H. Kageyama, O. Nakamura, J. Power Sources 68 (1997) 623.
[16] C. Masquelier, M. Tabuchi, K. Ado, R. Kanno, Y. Kobayashi, Y. Maki, O. Nakamura, J.B. Gooodenough, J. Solid State Chem. 123 (1996) 255.

[17] Y. Shimakawa, T. Numata, J. Tabuchi, J. Solid State Chem. 131 (1997) 138.
[18] P. Endres, B. Fuchs, S. Kemmler-Sack, K. Brandt, G. Faust-Becker, H.-W. Praas, Solid State Ionics 89 (1996) 221.
[19] J.C. Hunter, J. Solid State Chem. 39 (1981) 142.
[20] F. Izumi, The Rietveld Method, in: R.A. Young (Ed.), Oxford Univ. Press, Oxford, 1993, pp. 236–239, Chap. 13.
[21] R. Kanno, A. Kondo, M. Yonemura, R. Gover, Y. Kawamoto, M. Tabuchi, T. Kamiyama, F. Izumi, C. Masquelier, G. Rousse, J. Power Sources 81–82 (1999) 542.
[22] R. Kanno, M. Yonemura, T. Kohigashi, Y. Kawamoto, M. Tabuchi, T. Kamiyama, J. Power Sources 97–98 (2001) 423.
[23] G. Li, Y. Iijima, Y. Kudo, K. Brandt, H. Azuma, Solid State Ionics 146 (2002) 55.